Absorption Spectrum of OH Radical in Water

Daniel M. Chipman

Radiation Laboratory, University of Notre Dame, Notre Dame, Indiana 46556-5674

Received: August 18, 2008; Revised Manuscript Received: October 3, 2008

The influence of water on the ultraviolet absorption spectrum of OH radical is investigated with electronic structure calculations. One purpose of the work is to benchmark computational methods for their ability to treat this problem. That is done by applying a number of methods to characterization of the excited states of a variety of arrangements having OH interacting with one H_2O molecule. In high-level coupled-cluster approaches, it is found that triple excitations are of considerable importance. Two promising methods based on highly efficient time-dependent density functional theory are identified that may provide qualitatively useful results, but no method is found that is both efficient and capable of providing quantitative accuracy. Another purpose of the work is to suggest a plausible interpretation of the experimental absorption spectrum of aqueous OH radical. For this purpose an accurate coupled cluster approach is applied to the various $OH \cdot H_2O$ structures considered, along with a dielectric continuum representation of the further effects of additional bulk water. The valence transition localized on OH that is found at ~300 nm in gas is found to be considerably broadened by hydrogen bonding interactions with water. These transitions are assigned to the very broad shoulder on the experimental aqueous spectrum that extends from ~300 to 400 nm. The main experimental aqueous absorption band peaking at ~230 nm is found to arise instead mainly from rare hemibonded structures, which contribute out of proportion to their relative populations by virtue of having large oscillator strengths. The region near the experimental peak and on its blue side is primarily due to charge transfer transitions that move an electron to OH from hemibonded water, while the region on the near red side of the peak is primarily due to valence transitions localized on OH that is interacting with hemibonded water.

Introduction

The OH radical is an ubiquitous oxidizing agent formed in the radiation chemistry of liquid water.[1,2] It is also important in many aqueous reactions involving biological processes[3] and environmental remediation.[4] Consequently, detailed kinetics have been determined for many OH radical reactions in water.[5] These kinetics can often be advantageously monitored by following the time dependence of the ultraviolet (UV) absorption spectrum of aqueous OH radical.[6−9] It may be surprising, therefore, that this spectrum has never been definitively assigned.

The UV spectrum of OH in water was first identified[10] as a broad band in the 200−300 nm region, and subsequently established[11−14] to have a maximum at ~230 nm. A detailed and precise measurement[14] showed that in addition to the main band there is also a distinct shoulder of the spectrum in the 300−400 nm range.

Two studies[15,16] on the temperature dependence from 20 to 200 °C of the OH spectrum in water showed very little change of the position of the band maximum or of the band shape near the maximum, and concluded that the molar absorption coefficient must remain essentially constant over that temperature range. One of those studies[15] also noted that the absorption above 300 nm seems to increase with temperature, although the possibility of that being an artifact was not ruled out. A very recent work[9] has provided much more detail on the OH absorption spectrum in water over the temperature range 25−350 °C. In contrast to earlier works,[15,16] the molar absorption coefficient measured in the 250−290 nm region was found to decrease significantly with temperature. At the same time, a weak band at about 310 nm was found to grow in with temperature.

The experimental absorption spectrum of OD in D_2O has been compared[13] with that of OH in H_2O at ambient conditions, reporting the two spectra to be identical within experimental error in the 210−260 nm region. Another study[17] of the OD spectrum found its shape in the 220−320 nm region to be identical, within experimental error, at temperatures of 17.5 and 200 °C, and further found that the molar absorption coefficient at 250 nm is the same for OD and OH within experimental error.

To interpret these observed spectra in water, it is helpful to consider the situation of OH in the gas phase. Experimental observations on gas phase OH find the transition from the ground state $\tilde{X}$ ($^2\Pi_i$) to the lowest excited state $\tilde{A}$ ($^2\Sigma^+$) at 309 nm.[18] All higher excited states lie at quite high energy, being well under 200 nm.[18−20] For convenience, this valence $\tilde{A} \leftarrow \tilde{X}$ transition in free OH, which remains similar and highly localized on OH in its clusters with water, will be referred to simply as the AX transition in the remainder of this work.

It is also relevant to consider what is known about the spectrum of OH in water ice. Experimental observations[21,22] of the UV absorption spectrum of OH radical in ice have been interpreted in terms of two different absorbing species. One work[21] identified a single broad band attributed to OH, having maximum at about 280 nm and a long blue tail extending below 230 nm. This band was postulated to be due to OH trapped in substitutional sites and hydrogen bonded to adjacent water molecules. Another work[22] carried out under different conditions also identified a single broad band attributed to OH, but having maximum at about 245 nm. The latter workers interpreted their 245 nm band as due to OH trapped in substitutional sites and hydrogen bonded to adjacent water molecules, therefore having a spectrum similar to that found in liquid water. They also

10.1021/jp807399b CCC: $40.75
Published on Web 11/20/2008

reinterpreted the earlier observed[21] 280 nm band as being instead due to OH trapped in interstitial sites with little or no hydrogen bonding to water, therefore having a spectrum similar to that found in gas.

Trenin and Hayon[23] have argued that the main 230 nm absorption of OH radical in liquid water is blue-shifted too much (about 1.4 eV) from the gas phase to be attributed to simple solvent perturbation of the AX transition. Instead, it was proposed that the 230 nm band is due to an entirely different transition produced by charge transfer in the excited state, with a nearby solvent water molecule as electron donor and the OH radical as electron acceptor. Some calculations were put forth to support this assignment. Delahay[24] accepted without comment the charge transfer interpretation of the 230 nm band, and correlated the charge transfer energy with the energetics of photoelectron emission. We refer to this "charge transfer from solvent" transition simply as the CT transition in the remainder of this work.

The general idea of charge transfer spectra is an old one. Mulliken[25] described and applied a qualitative molecular orbital theory for the situation of a Lewis base forming a complex with a Lewis acid, both partners having closed shell ground states, and an excitation then corresponding to partial transfer of an electron from the base to the acid. Later the theory was adapted[26] for the situation that the partners are in contact by virtue of random encounters, without the requirement that they form a stable ground state complex. The idea of a vertical excited state produced by transfer of essentially a whole electron from a closed shell solvent molecule into the valence hole of a radical solute has been invoked to explain the observed spectra of I atom,[23,24,27−29] of NO,[30] of Cl, Br, OH, and H,[23,24] and of Fe^{3+} and Ce^{4+}.[24]

Nielsen, Michael, and Hart[13] claimed that the ∼230 nm absorption band of OH radical in water is in fact due to the AX transition, with the large blue shift from gas being due to hydrogen bonding interactions of the radical with water. These workers suggested that the charge transfer interpretation proposed by Trenin and Hayon[23] for aqueous OH should instead be applied to a different and higher energy band that peaks under 200 nm.

In their experimental study on the temperature dependence of the aqueous OH radical absorption spectrum Janik, Bartels, and Jonah[9] interpreted the main 230 nm band of OH radical in water as due to absorption by hydrogen bonded OH radicals, and the shoulder at 300 nm and above as a separate band due to free or non-hydrogen bonded OH, without being specific about the detailed nature of the transitions involved.

Very high level ab initio calculations[31,32] have been carried out on the ground and lowest excited states of OH complexed with one H_2O molecule as arranged in the most stable structure, with OH acting as a H-bond donor to H_2O. Interestingly, the AX vertical transition in this complex was found to be red-shifted with respect to free OH by about 0.4 eV, pushing it up to about 330 nm. A large structural change is found in the excited state, indicating that the spectrum of the complex may be broad and featureless.

Recently Tsai, Kowalski, Valiev, and Dupuis[33] carried out high-level ab initio and time-dependent density functional theory calculations on various clusters of OH complexed with one through seven H_2O molecules and of OH complexed with 16 H_2O molecules arranged in any of four different hydrogen bonding patterns. In all cases CT transitions were found in the region of the experimental maximum, these being weak in nearly all cases except for one of the $OH(H_2O)_{16}$ clusters that showed a very strong CT transition at ∼250 nm. On that basis it was concluded that the experimental absorption found near 230 nm for aqueous OH can be assigned to CT transitions.

In this work we complement the studies discussed above in two ways. We evaluate a number of computational methods to treat vertical excited states of an OH radical interacting with one H_2O molecule in a variety of different arrangements, in an effort to find accurate yet efficient methods that may be used in more extensive future studies on larger clusters. We also select an accurate method and augment it with a dielectric continuum representation of additional bulk water effects to obtain more detailed insight into how different kinds of interactions between OH and H_2O may contribute to different regions of the UV absorption spectrum of aqueous OH.

The paper is organized as follows. First, additional background necessary to discuss the detailed electronic structures of OH and H_2O is provided. After that a preliminary screening of a number of computational methods is carried out based on their performance on free OH and on three selected symmetric $OH\cdot H_2O$ structures. Then feasible and useful approaches are identified and subjected to additional screening based on their performance on a larger class that further includes 13 nonsymmetric $OH\cdot H_2O$ structures. The highest level computational method that remains feasible for all the structures is then used, along with dielectric continuum corrections, to propose a plausible interpretation of the aqueous OH absorption spectrum. Finally, a brief conclusion is supplied.

Background

The $\tilde{X}$ ($^2\Pi_i$) ground state of a free OH radical is doubly degenerate, neglecting spin−orbit effects. The nominal valence electronic configuration is $\sigma_{lp}^2\,\sigma_b^2\,\pi^3$, where σ_{lp} is the lone pair orbital lying along the molecular axis, σ_b is the O−H bonding orbital, and π represents the shell of two equivalent oxygen p-orbitals lying perpendicular to the molecular axis. The degeneracy arises from the two possible ways of orienting the single hole in the incomplete π valence shell. When an OH radical approaches an H_2O molecule this degeneracy is lifted and the two possible hole states that descend from the π shell of free OH then have different energies. However, this energy splitting generally remains small so that transition to the first excited state that is obtained by switching the hole in the putative π shell of OH remains in the infrared region.

The next state of a free OH radical is $\tilde{A}$ ($^2\Sigma^+$), which has electronic configuration $\sigma_{lp}^2\,\sigma_b^1\,\pi^4$. In gas phase OH the valence AX transition energy has an electronic contribution of 4.05 eV (306 nm),[18] which differs only slightly from the 4.02 eV (309 nm) actually observed[18] for the 0−0 transition that includes zero-point vibrational contributions. After that the excited states of free OH lie at very high energy. The dipole forbidden $\tilde{1}$ ($^2\Sigma^-$) state has been calculated to lie at ∼172 nm[75] or ∼157 nm,[20] and the allowed $\tilde{B}$ ($^2\Sigma^+$) state is found to lie at under 144 nm.[18]

The ground state of a free H_2O molecule has a valence electronic configuration $\sigma_{lp}^2\,\sigma_b^2\,\sigma_{b'}^2\,\pi^2$, where σ_{lp} is the lone pair orbital in the molecular plane, σ_b and $\sigma_{b'}$ are symmetry adapted linear combinations of the two O−H bonding orbitals, and π is the lone pair oxygen p-orbital lying perpendicular to the molecular plane. Transition to the lowest singlet excited state of a free H_2O molecule has band maximum at about 166 nm.[34] This excited state has partial Rydberg character, and is consequently blue-shifted to even higher energy at about 151 nm[35] in liquid water, and consequently does not overlap the OH absorption spectrum that is of interest in this work.

For a gas phase OH radical separated by a very large distance from a H_2O molecule, one can readily obtain the energy that

would produce a vertical CT excited state with electronic configuration of $OH^-(\sigma_{lp}^2\ \sigma_b^2\ \pi^4) + H_2O^+(\sigma_{lp}^2\ \sigma_b^2\ \sigma_b'^2\ \pi^1)$. Combining the first ionization potential of H_2O[36] with the electron affinity of OH[37] gives a very high energy corresponding to a wavelength of 115 nm for the lowest vertical CT transition of otherwise noninteracting OH + H_2O. If the two ions are brought into close proximity, the further inclusion of their mutual attraction as roughly estimated by the Coulomb energy of two point charges leads to a CT transition wavelength of 213 nm if the charges are separated by 2.9 Å, or to 246 nm if the charges are separated by 2.5 Å. Furthermore, solvation by other water molecules would lead to additional stabilization of the highly polar CT excited state. It is therefore not at all unreasonable to consider the possibility of CT transitions contributing to the UV absorption spectrum of OH in water.

We summarize this brief survey by noting the main candidates for transitions that might be expected to occur in the 200−400 nm region, which is the region of primary interest in the present work. Among the various intramolecular OH or H_2O gas phase transitions, only AX occurring near 300 nm is a reasonable candidate. Another possibility is that the intermolecular CT transition that is very high energy in the gas phase might be lowered considerably into the UV region when OH and H_2O come into contact in aqueous solution. All other transitions would appear to be either too low or too high in energy to contribute to the observed 200−400 nm spectrum, and that speculation is confirmed in the present work.

Computational Methods

Several computational methods are utilized for the electronic structure calculations reported in this work. A frozen core approximation is assumed thoughout.

The simplest method used is denoted CIS[38,39] (spin-unrestricted configuration interaction with single excitations). Closely related are TDDFT[40,41] (spin-unrestricted time-dependent density functional theory) methods taken within the TDA (Tamm-Dancoff) approximation,[42] here using the functionals B3LYP,[43,44] BHandH,[45,46] and MPW1K.[47] Henceforth we refer to these TDDFT(TDA) methods simply by the names of the functionals involved. These methods are all used as they are implemented in the NWChem computer program,[48] version 5.0.

A MR(2)-SDTCI (multireference space having two configurations, followed by single, double, and triple excitation configuration interaction) method was used as implemented in the Gamess[49] program. This approach starts with a MCSCF (multiconfiguration self-consistent-field) procedure to produce spin-restricted orbitals from a state average of the two lowest nearly degenerate states. This is followed by a configuration interaction based on an occupation-restricted multiple active space approach,[50,51] which includes all configurations that can be generated with the 15 valence electrons by placing 9−12 electrons in the six doubly occupied MCSCF valence orbitals, 0−4 electrons in the two partially occupied and nearly degenerate MCSCF orbitals, and 0−3 electrons in all the remaining virtual MCSCF orbitals.

Coupled cluster methods[52,53] were used at several levels of sophistication, as implemented in the NWChem computer program.[48] All are based on spin-unrestricted EOM (equations-of-motion) approaches for generating excited states. The reference states for all systems considered were found to have total spin $\langle S^2 \rangle$ from 0.750 to 0.760, and exploratory calculations using spin-restricted coupled cluster methods consistently gave very nearly the same results as with the corresponding unrestricted methods, so spin contamination is not a significant issue. Methods labeled EOM-CCSD (coupled clusters with iterative single and double excitations), EOM-CCSD(T)-IA[54,55] (EOM-CCSD plus noniterative triple excitations in the IA approximation), and EOM-CCSDT (EOM-CCSD plus iterative triple excitations) were all considered. The EOM-CCSD(T)-IA excited state results were referenced to CCSD(T)[56] ground state energies, rather than to the CCSD ground state energies as reported by the NWChem program, because use of the latter reference led in some cases to unphysical negative energies for transitions between the two lowest and nearly degenerate states.

Two different basis sets were utilized. The smallest one is designated as 6-311(2+)G*, which is based on the standard 6-311+G* basis set[57−60] that is triple-ζ in the sp-valence space also with sp-diffuse functions and d-polarization functions on oxygen, and then further augmented with a second shell of oxygen sp-diffuse functions obtained by simple geometric progression with a division factor of 3.32. That basis proved satisfactory in our previous studies on the lowest neutral excited states[61,62] and Feshbach anionic states[63] of water clusters.

For reference purposes the large aug-cc-pVTZ (augmented correlation-consistent polarized valence triple-ζ) basis set[64,65] that is of triple-ζ quality in the sp-valence space with dd′f-polarization functions on oxygen, pd-polarization functions on hydrogen, and augmented with spdf-diffuse functions on oxygen and spd-diffuse functions on hydrogen, was used where it was feasible.

In some cases a method labeled "EOM-CCSDT/aug-cc-pVTZ" was constructed to estimate the result of a true EOM-CCSDT/aug-cc-pVTZ calculation. This was done by separately adding to the EOM-CCSD/6-311(2+)G* result a correction for full iterative triple excitations, as obtained by comparison to EOM-CCSDT/6-311(2+)G*, and another correction for basis set extension, as obtained by comparison to EOM-CCSD/aug-cc-pVTZ.

Some rough estimates of the nonspecific effects of bulk water on transition free energies of the OH·H_2O solute complexes were made using simple dielectric continuum theory with the classical formula[66,67]

$$\Delta E = -[f(\epsilon)\mu \cdot \Delta\mu + f(n^2)\Delta\mu \cdot \Delta\mu/2]/R^3 \qquad (1)$$

where R is the solute cavity radius, μ is the ground state dipole moment vector, $\Delta\mu$ is the change in dipole moment vector upon passing to the excited state, $\epsilon = 78.4$ is the static solvent dielectric constant, $n^2 = 1.777$ is the square of the solvent refractive index, and $f(x) = 2(x - 1)/(2x + 1)$.

Determination of a proper value for the cavity radius R is problematic. In part this is because there is no generally accepted definition of R even for a spherical solute, and that is exacerbated in the present situation because an OH·H_2O solute complex is not spherical. A reasonable definition of the solute volume is easier to come by, and for this we opt to use the volume enclosed by the 0.001 e/a_0^3 isodensity contour of the unrestricted Hartree−Fock ground state wave function, as obtained from the Gamess program. A sphere encompassing that same volume then serves to produce an effective radius of the complex. All the OH·H_2O complexes considered in this work turn out to have effective radii determined from this criterion of 2.2−2.4 Å. For consistency we adopt the average value 2.3 Å for all the complexes. Finally we add to that an additional 0.7 Å, which is roughly half the diameter of a water molecule, to account for the finite size of the first-shell water molecules, leading to a common value of 3.0 Å that is used to estimate the cavity radii of all the OH·H_2O complexes. The calculated energy shift is not overly sensitive to this choice. For example, a change in

this value of R by as much as 0.2 Å leads to a change of only about 20% in ΔE. Even so, because of both the simplicity of the model and uncertainty in the choice of R, this procedure should be regarded as indicative only of the sign and approximate magnitude of nonspecific bulk water effects.

We report in this work only those transitions whose calculated energies fall within a certain window of interest. Thus, transitions to the very low energy first excited state of OH, which is degenerate with the ground state in the gas phase, are calculated in all the structures to lie in the infrared region of under 0.80 eV (1500 nm), and are omitted. As an upper bound, all remaining excited states are reported that have calculated energy up to 6.20 eV (200 nm). No corrections are made for the small vibrational or very small rotational contributions, so that only the electronic contributions to transition energies are reported. Oscillator strengths and dipole moment changes upon excitation are also reported in those cases where they are available from the program outputs.

Evaluation of Computational Methods

Description of Symmetric Structures. We first consider a variety of computational methods for free OH radical at its experimental equilibrium geometry[18] and for three representative structures of $OH\cdot H_2O$ complexes taken from a literature calculation carried out by Cabral do Couto et al.[68] The three $OH\cdot H_2O$ structures, here labeled C1, C3, and C2 to maintain consistency with the literature, were optimized with the MPW1PW91[69] density functional using the aug-cc-pVDZ[64,65] basis set. By taking advantage of the small size of free OH and of the plane of symmetry that exists in the C1, C3, and C2 structures of $OH\cdot H_2O$, we are able to carry out higher level calculations than would otherwise be feasible. These structures are utilized in this section to identify suitable lower level computational methods that can then be applied later below to other structures of $OH\cdot H_2O$ having no spatial symmetry, as well as to larger clusters in future work.

The C1, C3, and C2 structures are depicted in Figure 1 and significant parameters of the structures are included in Table 1, together with other structures that will be discussed later. The binding energies in Table 1 are calculated at the CCSD(T)/6-311(2+)G* level of theory, and include counterpoise correction[70] for basis set superposition errors (BSSE). They are in semiquantitative agreement with the MPW1PW91 results,[68] and the C1 binding energy agrees very well with the value −6.0 kcal/mol obtained from a high-level ab initio literature calculation.[71]

Among $OH\cdot H_2O$ structures, C1 is the global minimum with OH acting as a hydrogen bond donor to H_2O. Structure C3 is a local minimum with OH acting as a hydrogen bond acceptor from H_2O. Structure C2 is a local minimum at the MPW1PW91/aug-cc-pVDZ level of theory with OH being hemibonded to H_2O, wherein a two-center three-electron σ bond forms by overlap of the singly occupied π orbital on OH and the doubly occupied π orbital on a nearby favorably oriented H_2O. However, hemibonded structure C2 is not found to be a local minimum at higher levels of theory, and probably occurs as a stationary point in optimizations with many common density functionals only because of overbinding due to self-interaction errors.[72] In any event, our high-level calculation on the binding energy (see Table 1) shows structure C2 to be significantly more stable than dissociated $OH + H_2O$, so it remains an interesting structure for consideration.

Results for AX Transitions. Excited state information obtained at a variety of computational levels for each of these structures is reported for AX transitions in Table 2. For free OH the "EOM-CCSDT/aug-cc-pVTZ" result is only 0.01 eV higher than the EOM-CCSDT/aug-cc-pVTZ result and only 0.08 eV higher than experiment.[18] For structure C1 the "EOM-CCSDT/aug-cc-pVTZ" result is only 0.05 eV below a high-level CC3/aug-cc-pVTZ computational result in the literature.[32] Furthermore, most of this latter small difference is due to the slightly different geometry used, as can be seen by comparison of our EOM-CCSD/aug-cc-pVTZ result with that reported for the same method in ref 32. These comparisons give support to

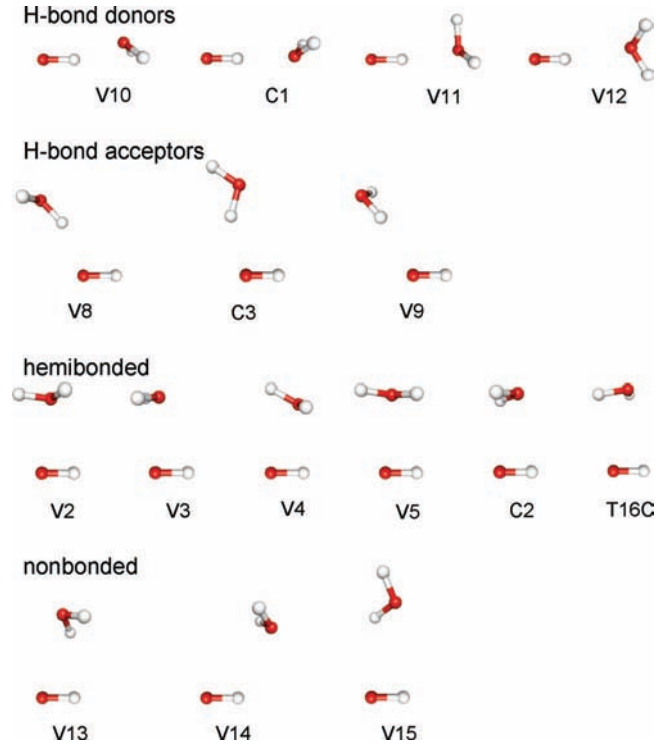

Figure 1. Depictions of $OH\cdot H_2O$ structures.

TABLE 1: Geometric Data and Calculated Binding Energy for all $OH\cdot H_2O$ Structures[a]

structure	R(O···O)	R(H···O)	binding energy
H-bond donor structures			
V10	2.750	1.757	0.8
C1	2.854	1.870	−6.1
V11	3.000	1.956	1.2
V12	3.100	2.165	−3.8
H-bond acceptor structures			
V8	2.850	1.882	7.2
C3	2.936	2.025	−3.2
V9	2.950	2.058	−0.4
hemibonded structures			
V2	2.300		3.0
V3	2.350		5.8
V4	2.400		6.1
V5	2.450		3.8
C2	2.467		−2.1
T16C	2.722		−3.5
nonbonded structures			
V13	3.400		3.8
V14	3.600		−1.4
V15	3.700		4.7

[a] O···O and hydrogen bonded H···O distances are in Å. Binding energies relative to separated $OH + H_2O$ are in kcal/mol, as calculated with the CCSD(T)/6-311(2+)G* method with correction for BSSE.

TABLE 2: AX Transitions Calculated by Various Methods for OH and for Several OH·H$_2$O Structures[a]

method	ΔE	λ	f	$\lvert\Delta\mu\rvert$
free OH				
CIS	4.72	263	0.0045	0.2
B3LYP	4.40	282	0.0042	
BHandH	4.29	289	0.0042	
MPW1K	4.48	277	0.0043	
MR(2)-SDTCI	4.29	289		0.2
EOM-CCSD	4.31	288	0.0040	0.2
EOM-CCSD(T)-IA	4.34	286		
EOM-CCSDT	4.30	288	0.0039	0.2
EOM-CCSD/aug-cc-pVTZ	4.14	299	0.0016	0.1
"EOM-CCSDT/aug-cc-pVTZ"	4.13	300		
EOM-CCSDT/aug-cc-pVTZ	4.12	301	0.0015	0.04
Experiment[b]	4.05	306	0.0013	
H-bond donor structure C1				
CIS[c]	4.30	289	0.0038	5.3
B3LYP	3.69, 5.08	336, 244	0.0030, 0.0033	
BHandH	3.82	325	0.0034	
MPW1K	3.99	310	0.0034	
MR(2)-SDTCI	3.95	314		0.6
EOM-CCSD	3.85	322	0.0034	0.6
EOM-CCSD(T)-IA	4.00	310		
EOM-CCSDT	3.83	324	0.0033	0.7
EOM-CCSD/aug-cc-pVTZ	3.73	332	0.0017	0.6
"EOM-CCSDT/aug-cc-pVTZ"	3.71	334		
CC3/aug-cc-pVTZ[d]	3.76	330	0.0018	
H-bond acceptor structure C3				
CIS	4.72	263	0.0038	1.8
B3LYP	3.79, 4.45	327, 279	0.0001, 0.0034	
BHandH	4.28	290	0.0035	
MPW1K	4.47	278	0.0035	
MR(2)-SDTCI	4.39	283		0.2
EOM-CCSD	4.30	288	0.0032	0.2
EOM-CCSD(T)-IA	4.45	278		
EOM-CCSDT	4.29	289	0.0031	0.2
EOM-CCSD/aug-cc-pVTZ	4.14	299	0.0013	0.03
"EOM-CCSDT/aug-cc-pVTZ"	4.13	300		
hemibonded structure C2				
CIS	4.92	252	0.0042	1.4
B3LYP	5.63	220	0.0095	
BHandH	4.49	276	0.0017	
MPW1K	4.65	266	0.0005	
MR(2)-SDTCI	4.62	268		0.1
EOM-CCSD	4.54	273	0.0021	0.1
EOM-CCSD(T)-IA	4.69	264		
EOM-CCSDT	4.53	274	0.0011	0.1
EOM-CCSD/aug-cc-pVTZ	4.41	281	0.0010	0.2
"EOM-CCSDT/aug-cc-pVTZ"	4.39	282		

[a] All methods reported use the 6-311(2+)G* basis set unless explicitly shown otherwise. Transition energy ΔE is in eV, wavelength λ is in nm, oscillator strength is f, and dipole moment change $\lvert\Delta\mu\rvert$ is in debye. [b] Energy from ref 18. Oscillator strength from ref 73. [c] Mixed AX and CT state. [d] Reference 32.

TABLE 3: CT Transitions Calculated by Various Methods for Several OH·H$_2$O Structures[a]

method	ΔE	λ	f	$\lvert\Delta\mu\rvert$
H-bond acceptor structure C3				
B3LYP	1.85	676	0.0071	
BHandH	4.98	249	0.0037	
MPW1K	4.49	246	0.0035	
MR(2)-SDTCI	5.06	245		10.8
EOM-CCSD	5.43	228	0.0028	12.5
EOM-CCSD(T)-IA	5.41	229		
EOM-CCSDT	4.68	265	0.0024	10.0
EOM-CCSD/aug-cc-pVTZ	5.56	223	0.0035	12.3
"EOM-CCSDT/aug-cc-pVTZ"	4.81	258		
hemibonded structure C2				
B3LYP	4.07, 4.64	305, 267	0.1145, 0.0392	
BHandH	5.73	216	0.1073	
MPW1K	5.45	228	0.1107	
MR(2)-SDTCI	5.71	217		8.0
EOM-CCSD	5.82	213	0.0934	9.0
EOM-CCSD(T)-IA	5.89	211		
EOM-CCSDT	5.36	231	0.0883	8.6
EOM-CCSD/aug-cc-pVTZ	5.88	211	0.0876	8.8
"EOM-CCSDT/aug-cc-pVTZ"	5.42	229		

[a] All methods reported use the 6-311(2+)G* basis set unless explicitly shown otherwise. Transition energy ΔE is in eV, wavelength λ is in nm, oscillator strength is f, and dipole moment change $\lvert\Delta\mu\rvert$ is in debye.

"EOM-CCSDT/aug-cc-pVTZ", which is the highest level method available for all the structures considered in this section, being quite reliable. It is therefore taken as a reference standard, and for consistency the other lower level methods will all be evaluated below to determine errors with respect to the "EOM-CCSDT/aug-cc-pVTZ" results.

The CIS/6-311(2+)G* method performs poorly, giving errors from 0.53 to 0.59 eV too high. For structure C1, examination of the wave function and of the dipole moment change indicates a significant degree of spurious mixing with the CT state.

The TDDFT(TDA) methods show mixed performance. The B3LYP/6-311(2+)G* method is poor having a very large spread of errors ranging from 0.06 eV too low to 1.21 eV too high, the BHandH/6-311(2+)G* method is quite good having a narrow range of errors from 0.10 to 0.16 eV too high, and the MPW1K/6-311(2+)G* method is satisfactory having errors from 0.26 to 0.35 eV too high.

The MR(2)-SDTCI/6-311(2+)G* method also performs satisfactorily, having a very narrow range of errors from 0.23 to 0.24 eV too high.

The various EOM-CC methods are also all satisfactory, with EOM-CCSD/6-311(2+)G* having a narrow range of errors from 0.14 to 0.18 eV too high, EOM-CCSD(T)-IA/6-311(2+)G* having errors from 0.22 to 0.32 too high, and EOM-CCSDT/6-311(2+)G* having a narrow range of errors from 0.12 to 0.17 eV too high.

Comparison between the EOM-CCSD/6-311(2+)G* and EOM-CCSDT/6-311(2+)G* results indicates that triple excitations are of little importance, lowering the excitation energy by only 0.0−0.02 eV. Comparison between EOM-CCSD/6-311(2+)G* and EOM-CCSD/aug-cc-pVTZ results indicates that basis set extension is a more important effect, lowering the excitation energy by 0.12−0.30 eV.

Among the methods for which oscillator strengths and dipole moment changes are available, all except for CIS/6-311(2+)G* give similar results to one another, with oscillator strengths from 0.001 to 0.004 and $\lvert\Delta\mu\rvert$ under 2.0 debye.

Results for CT Transitions. Excited state information obtained at a variety of computational levels for each of these structures is reported for CT transitions in Table 3 These are readily identified by unmistakeable indications of $OH^-\cdot H_2O^+$ character in the excited state wave functions and/or by finding very large excited state dipole moments. Our highest level "EOM-CCSDT/aug-cc-pVTZ" results are used here as the best available references for comparison. They indicate that structure C1 does not have a CT state in the window of interest, while structures C3 and C2 each have one such state.

The CIS/6-311(2+)G* method performs very poorly, inappropriately omitting any results in the window of interest for structures C3 and C2.

The TDDFT(TDA) methods again show mixed performance. The B3LYP/6-311(2+)G* method performs poorly, inappropriately placing a result in the window of interest for structure C1 and inappropriately placing two (instead of one) CT states in the window of interest for both structures C3 and C2, in each case having one of these states being unphysically low in energy.

The BHandH/6-311(2+)G* method performs satisfactorily, giving results 0.17−0.31 eV too high. The MPW1K/6-311(2+)G* method also performs satisfactorily, giving results 0.32 eV too low to 0.03 eV too high.

The MR(2)-SDTCI/6-311(2+)G* method also performs satisfactorily, having errors from 0.25 to 0.29 eV too high, which is also quite consistent with the errors seen above for the AX transition.

The various EOM-CC methods show mixed performance, with EOM-CCSD/6-311(2+)G* being poor having errors from 0.40 to 0.62 eV too high, EOM-CCSD(T)-IA/6-311(2+)G* also being poor having errors from 0.47 to 0.60 too high, and EOM-CCSDT/6-311(2+)G* being good having a narrow range of errors from 0.06 to 0.13 eV too low.

Comparison between the EOM-CCSD/6-311(2+)G* and EOM-CCSDT/6-311(2+)G* results indicates that triple excitations are quite significant, lowering the excitation energy by 0.46−0.75 eV. Comparison between EOM-CCSD/6-311(2+)G* and EOM-CCSD/aug-cc-pVTZ results indicates that basis set extension has a modest effect, raising the excitation energy by 0.06−0.13 eV.

Among the methods for which oscillator strengths and dipole moment changes are available, the oscillator strengths are reasonably consistent, being near 0.003 for structure C3 and near 0.10 for structure C2, as are the dipole moment changes that are consistently near 10 debye for both structures.

Prognosis. The main purpose of this section is to carry out a preliminary screening to identify methods that may be satisfactory when used with the 6-311(2+)G* basis set, since calculations with the much larger aug-cc-pVTZ basis would not be feasible for large clusters with any of these methods. The CIS/6-311(2+)G* and B3LYP/6-311(2+)G* methods are found to perform poorly for both kinds of transitions considered. Most of the remaining methods give a more or less satisfactory description of AX transitions, but the CT transitions are more challenging.

Let us summarize the overall performance of methods with the 6-311(2+)G* basis set for both kinds of transitions, going from the most promising to the least satisfactory. The most consistently good method is EOM-CCSDT/6-311(2+)G*, with errors ranging from 0.13 eV too low to 0.17 eV too high. The BHandH/6-311(2+)G* method is also fairly good, with errors ranging from 0.10 to 0.31 eV too high. The MR(2)-SDTCI/6-311(2+)G* method is also fairly good, with quite consistent errors ranging from 0.25 to 0.29 eV too high. The MPW1K/6-311(2+)G* method has larger errors ranging from 0.32 eV too low to 0.35 eV too high. The remaining EOM-CCSD/6-311(2+)G* and EOM-CCSD(T)-IA/6-311(2+)G* methods have quite significant errors ranging up to 0.60 eV or more.

Further Evaluation of Selected Computational Methods

Description of Nonsymmetric Structures. To broaden the scope, we now consider a number of additional nonsymmetric structures of OH radical interacting with one H_2O molecule. The EOM-CCSDT/6-311(2+)G* method remains barely feasible for these calculations, and having been shown to be consistently good in the previous section will be used as a reference standard of comparison to further evaluate selected lower level methods. For the latter, we choose the very efficient and reasonably promising BHandH/6-311(2+)G* and MPW1K/6-311(2+)G* methods for further evaluation.

Most of these additional nonsymmetric structures were obtained from a first-principles molecular dynamics trajectory simulation carried out by VandeVondele and Sprik,[74] as taken from their calculation based on density functional theory with the BLYP functional. The simulation utilized 31 H_2O molecules and one OH radical, together with replication using periodic boundary conditions. They reported details on 15 extracted $OH\cdot H_2O$ structures, here labeled V1−V15 to maintain consistency with the literature. However, we omit three of those structures (V1, V6, and V7) from consideration because of their extremely unfavorable binding energies that we calculate to be $\geq$11 kcal/mol less stable than dissociated OH + H_2O at the CCSD(T)/6-311(2+)G* level with correction for BSSE.[70] The literature work[74] classified the remaining structures V10−V12 as having OH acting as an H-bond donor, V8−V9 as having OH acting as an H-bond acceptor, V2−V5 as being hemibonded, and V13−V15 as nonbonded structures. That classification is based on geometrical considerations, and is not meant to imply anything about the interaction energy between OH and H_2O. On the contrary, these structures were apparently selected to find OH and H_2O separated by certain predetermined distances, as seen in Table 1, and they should not be taken as a representative statistical sampling of likely structures.

It should be noted that while first-principles molecular dynamics simulations carried out on aqueous OH with the BLYP functional generally find hemibonding structures to be persistent,[74−77] all these works note that this finding may be an artifact of the well-known overbinding of such structures in density functional theory when no correction is made for self-interaction error. This notion was verified in the VandeVondele and Sprik study,[74] which also reported simulations using BLYP functionals that were modified in various ways to partially correct for the self-interaction error. After correction, hemibonded structrures were found to be only rare events in the simulations.

We also include one structure obtained from a literature calculation carried out by Tsai et al.,[33] who optimized a number of small $OH\cdot(H_2O)_n$ clusters with the MPW1K/6-31++G** method. They found one $OH\cdot(H_2O)_{16}$ cluster, named 16C, having OH in the interior and which exhibited an intense CT transition at ∼250 nm. Here we extract from that the $OH\cdot H_2O$ structure involving OH with the H_2O molecule identified by them as being responsible for the CT transition, and label it T16C. This structure corresponds to a hemibonding interaction.

The 13 nonsymmetric $OH\cdot H_2O$ structures considered are depicted in Figure 1 and significant parameters of the structures are included in Table 1. The binding energies calculated by CCSD(T)/6-311(2+)G* with BSSE correction reported in Table 1 are in semiquantitative agreement with the relative energies presented in Figure 1 of ref 74.

Further Results for AX and CT Transitions. Further results for AX transitions in the larger set of structures are reported in Table 4. Both the TDDFT(TDA) methods considered here perform fairly well. The BHandH/6-311(2+)G* method has errors ranging from 0.04 eV too small to 0.29 eV too high, but has a very narrow range of errors from −0.04 to 0.00 eV if structure V8 is omitted. The MPW1K/6-311(2+)G* method has errors ranging from 0.02 eV too small to 0.18 eV too high, with a number of structures showing errors in the 0.12 to 0.18 eV range.

Further results for CT transitions in the larger set of structures are reported in Table 5. The TDDFT(TDA) methods have more difficulty here, just as they did in the smaller set of symmetric structures. The BHandH/6-311(2+)G* method has errors ranging from 0.01 eV too small to 0.53 eV too high. The MPW1K/6-311(2+)G* method has errors ranging from 0.43 eV too small to 0.25 eV too high. Both methods have a somewhat narrower

TABLE 4: AX Transitions Calculated by Various Methods for OH and for All OH·H_2O Structures[a]

structure	BHandH ΔE	MPW1K ΔE	EOM-CCSDT ΔE (ΔE_{aq})	EOM-CCSDT λ (λ_{aq})	EOM-CCSDT f	EOM-CCSDT $\lvert\Delta\mu\rvert$
			free OH			
OH	4.29	4.48	4.30(4.29)	288(289)	0.0039	0.17
			H-bond donor structures			
V10	3.56	3.72	3.56(3.44)	348(360)	0.0024	1.20
C1	3.82	3.99	3.83(3.76)	324(330)	0.0033	0.72
V11	3.70	3.86	3.70(3.61)	335(343)	0.0024	1.13
V12	4.09	4.27	4.11(4.07)	302(305)	0.0041	0.44
			H-bond acceptor structures			
V8	4.45	4.29	4.16(4.32)	298(287)	0.0013	2.74
C3	4.28	4.47	4.29(4.29)	289(289)	0.0031	0.19
V9	4.15	4.13	4.15(4.24)	299(293)	0.0023	1.68
			hemibonded structures			
V2	4.82	4.98	4.85(4.86)	255(255)	0.0086	0.33
V3	4.64	4.79	4.67(4.67)	266(266)	0.0138	0.28
V4	4.44	4.60	4.48(4.48)	277(277)	0.0002	0.29
V5	4.67	4.84	4.69(4.69)	264(264)	0.0089	0.24
C2	4.49	4.65	4.53(4.53)	274(274)	0.0011	0.10
T16C	4.37	4.55	4.40(4.40)	282(282)	0.0031	0.20
			nonbonded structures			
V13	4.25	4.44	4.26(4.24)	291(292)	0.0032	0.28
V14	4.19	4.38	4.21(4.20)	295(295)	0.0028	0.21
V15	4.25	4.44	4.26(4.26)	291(291)	0.0035	0.22

[a] All calculations were carried out with the 6-311(2+)G* basis set. Transition energy ΔE is in eV, wavelength λ is in nm, oscillator strength is f, and dipole moment change $|\Delta\mu|$ is in debye.

TABLE 5: CT Transitions Calculated by Various Methods for All OH·H_2O Structures[a]

structure	BHandH ΔE	MPW1K ΔE	EOM-CCSDT ΔE (ΔE_{aq})	EOM-CCSDT λ (λ_{aq})	EOM-CCSDT f	EOM-CCSDT $\lvert\Delta\mu\rvert$
			H-bond acceptor structures			
V8	3.97	3.82	3.76(4.05)	330(306)	0.0007	8.15
C3	4.98	4.49	4.68(4.48)	265(277)	0.0024	11.12
V9	4.72	4.45	4.56(4.85)	272(256)	0.0007	10.06
			hemibonded structures			
V2	6.25	6.00	5.78(5.53)	214(224)	0.0748	6.55
V3	5.83	5.59	5.39(5.13)	230(242)	0.0836	7.47
V4	6.29	6.02	5.77(5.42)	215(229)	0.0670	7.24
V5	5.94	5.65	5.55(5.26)	224(236)	0.0646	8.06
C2	5.73	5.45	5.36(5.10)	231(243)	0.0883	8.61
T16C	5.77	5.42	5.53(5.20)	224(239)	0.0436	9.92
			nonbonded structure			
V13	5.98	5.56	5.99(5.74)	207(216)	0.0122	10.85

[a] All calculations were carried out with the 6-311(2+)G* basis set. Transition energy ΔE is in eV, wavelength λ is in nm, oscillator strength is f, and dipole moment change $|\Delta\mu|$ is in debye.

range of errors, becoming 0.16 to 0.53 eV and −0.19 to 0.25 eV, respectively, if the main outlier of structure V13 is omitted.

It can be concluded that the BHandH/6-311(2+)G* and MPW1K/6-311(2+)G* methods may be suitable for qualitative study of the aqueous OH radical UV spectrum, but neither is capable of delivering suitably quantitative results for the contributions from CT transitions. We await the development of efficient yet accurate methods, such as may well soon come from improved functionals for TDDFT(TDA) calculations, for subsequent progress on this problem. The benchmarks reported here should also prove useful to evaluate other promising methods in the future.

Implications for the Experimental OH Absorption Spectrum

Choice of Method. In this section we discuss our results from the EOM-CCSDT/6-311(2+)G* method to propose a plausible interpretation of the experimental UV absorption spectrum of aqueous OH radical. Excitation results from EOM-CCSDT/6-311(2+)G* calculations, together with estimated dielectric continuum corrections, are listed for AX transitions in Table 4 and for CT transitions in Table 5. Results that include dielectric continuum corrections are indicated with an "aq" subscript.

To aid discussion the results are also displayed in Figure 2, wherein the top panel shows AX transitions and the bottom panel shows CT transitions. The solid sticks in Figure 2 show the position of each transition as calculated in gas, and the dashed extension indicates its shift upon including the dielectric correction. The dashes are slanted, instead of being horizontal, simply to improve readibility. Note particularly in the bottom panel that the oscillator strengths for all CT transitions in hemibonded structures have been scaled down by an order of magnitude in order to fit them on the graphs.

Results for H-Bond Donors. The AX transition energies for structures classified as having OH acting as H-bond donor are red-shifted by 14−60 nm from that of free OH. The magnitude of this red shift shows a general although not perfect trend of increasing as the O···O distance decreases. The dielectric shifts

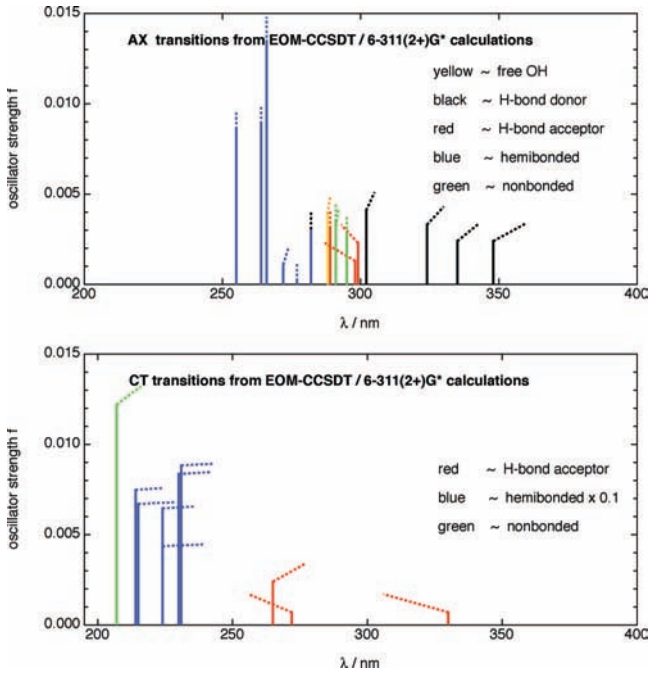

Figure 2. Calculated EOM-CCSDT/6-311(2+)G* transitions. The bottom part of each stick shows the position of the transition as calculated in gas, and the dashed line extension indicates its calculated dielectric shift. The top panel shows AX transitions, and the bottom panel shows CT transitions. The CT transitions in hemibonded structures are scaled down by a factor of 10.

are generally moderate, being 3−12 nm, and also all to the red. The oscillator strengths are similar in magnitude to that of free OH radical, while the dipole moment changes upon excitation are somewhat larger than those in free OH. The calculated transitions range from 302 to 348 nm for the free structures, changing slightly to 305 to 360 nm for the structures in dielectric. This places these absorptions throughout the region of the very wide shoulder above ~300 nm in the aqueous OH spectrum.

No CT transitions appear in the window of interest for these structures.

Results for H-Bond Acceptors. Compared to free OH, the AX transition energies for structures classified as having OH acting as an H-bond acceptor are red-shifted by 1−11 nm, the oscillator strengths are similar in magnitude, and the dipole moment changes upon excitation can be considerably larger. Dielectric shifts are moderate and to the blue, by amounts ranging from 0 to 9 nm. The calculated transitions range from 289 to 299 nm for the free structures, changing slightly to 287−293 nm for the structures in dielectric. This places these absorptions very near that of free OH, and near the weak band that develops at ~300 nm in the aqueous OH spectrum at high temperatures.[9]

The CT transitions have small oscillator strengths, comparable to those of the AX transitions, but have much larger dipole moment changes upon excitation, ranging from 8 to 11 debye. The calculated transitions in the free structures range from 272 to 330 nm. Note that structure V8 has its CT transition energy actually below that of its AX transition energy. These CT transitions all have significant dielectric shifts ranging from 12 nm to the red to 24 nm to the blue, which moves them to the range of 256−330 nm. This places these transitions over a wide range from the red side of the main peak in the aqueous OH spectrum out to the very wide shoulder above ~300 nm.

Results for Hemibonded Structures. The AX transition energies for structures classified as being hemibonded are all significantly blue-shifted from that of free OH by 6−33 nm, the oscillator strengths are usually but not always somewhat larger, and the dipole moment changes upon excitation are also usually but not always somewhat larger. The calculated transitions range from 255 to 282 nm for the free structures, and are essentially unaffected by the dielectric. This places them in the region on the red side of the main aqueous peak that occurs at about 230 nm.

The CT transitions have huge oscillator strengths ranging from 0.07 to 0.09, which is more than an order of magnitude larger than that of the AX transition in free OH, and also have very large dipole moment changes upon excitation ranging from 7 to 9 debye. The huge oscillator strength is a consequence of the favorable near-collinear alignment of the orbitals involved in the CT transitions, namely the valence π orbitals on OH and H_2O, when they are in a close hemibonding arrangement, allowing for a very large dipole transition moment to develop. The calculated transitions range from 214 to 231 nm for the free structures, being blue-shifted by 10−15 nm to range from 224 to 242 nm for the structures in dielectric. This places them in the region very near and slightly on the blue side of the main aqueous peak that occurs at ~230 nm.

Results for Nonbonded Structures. The AX transition energies for structures classified as being nonbonding are red-shifted from that of free OH by only 3−7 nm. The oscillator strengths and dipole moment shifts are also very similar to that of free OH. The dielectric shifts are essentially negligible. This places these absorptions very near that of free OH, and near the weak band that develops at ~300 nm in the aqueous OH spectrum at high temperatures.[9]

Only the V13 structure, which has the shortest O···O distance, shows a calculated CT transition in the window of interest, being at 207 nm, which just barely makes the cutoff criterion for inclusion. It has considerable oscillator strength and a large dipole moment change upon excitation. The dielectric shift is 9 nm to the red, which places it in a region to contribute on the far blue side of the main peak in the aqueous OH spectrum.

Interpretation of the OH Radical Spectrum in Bulk Water. To summarize for the AX transitions as compared to that in free OH, the H-bond donor structures are somewhat red-shifted, the H-bond acceptor structures are close or slightly red-shifted, the hemibonded structures are somewhat blue-shifted, and the nonbonded structures are hardly shifted at all. Most of these structures have oscillator strengths similar in magnitude to that of free OH, except that some hemibonded structures have considerably larger oscillator strengths. It can be concluded that the H-bond donor, H-bond acceptor, and nonbonded structures considered show AX transitions having energies in the same range as the long red tail of the aqueous OH spectrum shoulder at ~300 nm and above, while the hemibonded structures have energies in the region on the red side of the main aqueous peak that occurs at ~230 nm.

To summarize for the CT transitions, none are found in the window of interest for any of the H-bond donor structures, and it is found in only one of the three nonbonded structures examined, and there only at quite high energy. However, it is found in all the H-bond acceptor and hemibonded structures examined. In the H-bond acceptor structures the CT transitions contribute on the red side of the main aqueous peak all the way into the wide shoulder observed in the ~300−400 nm range. In the hemibonded structures the CT transitions contribute near to and on the blue side of the main aqueous peak and with very large oscillator strengths.

Conclusion

One purpose of this work is to benchmark computational methods for study of the aqueous OH radical UV absorption spectrum, in an effort to identify efficient yet accurate methods that can be used in future more elaborate studies on OH in large clusters of water molecules. Toward that end, extensive calculations were carried out with a number of different methods on free OH and on $OH \cdot H_2O$ structures.

A preliminary evaluation was made with calculations on free OH and just a few carefully selected $OH \cdot H_2O$ structures. All the methods tested generally performed well for AX transitions, but for two exceptions. However, widely varying performance ranging from poor to quite good was found for the more challenging CT transitions. Notably, in coupled cluster approaches it was found that triple excitations are of considerable importance.

On the basis of that preliminary survey, the promising and very efficient BHandH/6-311(2+)G* and MPW1K/6-311(2+)G* methods were selected for further evaluation on a larger collection of $OH \cdot H_2O$ structures. It was concluded that while the BHandH/6-311(2+)G* and MPW1K/6-311(2+)G* methods may be suitable for qualitative study of the aqueous OH radical spectrum, neither is adequate for quantitative treatment of the contributions from CT transitions.

High-level EOM-CCSDT/6-311(2+)G* results on the various $OH \cdot H_2O$ structures considered, together with dielectric continuum estimates of the influence of additional bulk water effects, were then used to propose an interpretation of the experimental UV absorption spectrum of aqueous OH radical. The broad main band observed experimentally to have a peak at ~230 nm seems to arise mostly from hemibonded configurations of OH with water. The intensity in the region near the peak and on its blue side comes primarily from hemibonded CT transitions, which have huge oscillator strengths and so contribute out of proportion to their relative likelihood. The red side of this peak comes primarily from hemibonded AX transitions that have large oscillator strengths, and to a lesser extent from CT transitions in H-bond acceptor structures. A band at ~300 nm that grows in at high temperatures is largely due to AX transitions in H-bond acceptor and nonbonded configurations. The broad shoulder extending through the ~300−400 nm range is largely due to AX transitions in the most stable H-bond donor structures.

This interpretation also suggests a qualitative explanation for the observed temperature dependence[9] of the aqueous OH radical spectrum. As temperature increases, the relative populations will shift away from any kind of bonded structures, and particularly from the already rare weakly bound hemibonded structures, and thereby cause the main peak found near 230 nm to diminish. At the same time the proportion of nonbonded structures will increase, causing a band near 300 nm to grow in at high temperatures.

To test these tentative conclusions, it would be useful to obtain a more extensive and more statistically representative sampling of structures from reliable molecular dynamics simulations, and also to carry out such simulations over a range of temperatures and pressures. More suitable methods should also be identified to perform accurate electronic structure calculations on extracted structures having many explicit H_2O molecules around the OH radical. With such larger clusters the possibility of the charge transfer electron coming from more than a single water molecule should be considered. Work on all these fronts is in progress.

Acknowledgment. We are grateful to Dr. P. Cabral do Couto, Dr. J. VandeVondele, and Dr. M. Dupuis, who generously provided geometrical coordinates for the various structures used in this work. Helpful discussions have been held with Dr. D. Bartels, Dr. I. Janik, Dr. I. Carmichael, and Dr. P. Cabral do Couto. The research described herein was supported by the Office of Basic Energy Sciences of the Department of Energy. This is Contribution No. NDRL-4774 from the Notre Dame Radiation Laboratory.

References and Notes

(1) Spinks, J. W.; Woods, R. J. *An Introduction to Radiation Chemistry*, 3rd ed.; J. Wiley and Sons: New York, 1990.
(2) Garrett, B. C.; Dixon, D. A.; Camaioni, D. M.; Chipman, D. M.; Johnson, M. A.; Jonah, C. D.; Kimmel, G. A.; Miller, J. H.; Rescigno, T. N.; Rossky, P. J.; Xantheas, S. S.; Colson, S. D.; Laufer, A. H.; Ray, D.; Barbara, P. F.; Bartels, D. M.; Becker, K. H.; Bowen, H.; Bradforth, S. E.; Carmichael, I.; Coe, J. V.; Corrales, L. R.; Cowin, J. P.; Dupuis, M.; Eisenthal, K. B.; Franz, J. A.; Gutowski, M. S.; Jordan, K. D.; Kay, B. D.; LaVerne, J. A.; Lymar, S. V.; Madey, T. E.; McCurdy, C. W.; Meisel, D.; Mukamel, S.; Nilsson, A. R.; Orlando, T. M.; Petrik, N. G.; Pimblott, S. M.; Rustad, J. R.; Schenter, G. K.; Singer, S. J.; Tokmakoff, A.; Wang, L. S.; Wittig, C.; Zwier, T. S. *Chem. Rev.* **2005**, *105*, 355.
(3) Halliwell, B.; Gutteridge, J. H. C. *Free Radicals in Biology and Medicine*, 3rd ed.; Oxford University Press: Oxford, UK, 1999.
(4) Pignatello, J. J.; Oliveros, E.; MacKay, A. *Crit. Rev. Environ. Sci. Technol.* **2006**, *36*, 1; **2007**, *37*, 273.
(5) Buxton, G. V.; Greenstock, C. L.; Helman, W. P.; Ross, A. B. *J. Phys. Chem. Ref. Data* **1988**, *17*, 513.
(6) Schmidt, K. H. *J. Phys. Chem.* **1977**, *81*, 1257.
(7) Elliott, A. J.; McCracken, D. R.; Buxton, G. V.; Wood, N. D. *J. Chem. Soc., Faraday Trans.* **1990**, *86*, 1539.
(8) Lundström, T.; Christensen, H.; Sehested, K. *Radiat. Phys. Chem.* **2002**, *64*, 29.
(9) Janik, I.; Bartels, D. M.; Jonah, C. D. *J. Phys. Chem. A* **2007**, *111*, 1835.
(10) Thomas, J. K.; Rabani, J.; Matheson, M. S.; Hart, E. J.; Gordon, S. *J. Phys. Chem.* **1966**, *70*, 2409.
(11) Pagsberg, P.; Christensen, H.; Rabani, J.; Nilsson, G.; Fenger, J.; Nielsen, S. O. *J. Phys. Chem.* **1969**, *73*, 1029.
(12) Boyle, J. W.; Ghormley, J. A.; Hochanadel, C. J.; Riley, J. F. *J. Phys. Chem.* **1969**, *73*, 2886.
(13) Nielsen, S. O.; Michael, B. D.; Hart, E. J. *J. Phys. Chem.* **1976**, *80*, 2482.
(14) Czapski, G.; Bielski, B. H. J. *Radiat. Phys. Chem.* **1993**, *41*, 503.
(15) Christensen, H.; Sehested, K. *Radiat. Phys. Chem.* **1981**, *18*, 723.
(16) Elliot, A. J.; Buxton, G. V. *J. Chem. Soc., Faraday Trans.* **1992**, *88*, 2465.
(17) Buxton, G. V.; Lynch, D. A.; Stuart, C. R. *J. Chem. Soc., Faraday Trans.* **1998**, *94*, 2379.
(18) Huber, K. P.; Herzberg, G. *Molecular Spectra and Molecular Structure. IV. Constants of Diatomic Molecules*; van Nostrand Reinhold: New York, 1979.
(19) van Dishoeck, E. F.; Dalgarno, A. *J. Chem. Phys.* **1983**, *79*, 873.
(20) Theodorakopoulos, G.; Petsalakis, I. D.; Buenker, R. J. *Chem. Phys. Lett.* **1987**, *138*, 71.
(21) Taub, I. A.; Eiben, K. *J. Chem. Phys.* **1968**, *49*, 2499.
(22) Ghormley, J. A.; Hochanadel, C. J. *J. Phys. Chem.* **1971**, *75*, 40.
(23) Treinin, A.; Hayon, E. *J. Am. Chem. Soc.* **1975**, *97*, 1716.
(24) Delahay, P. *Chem. Phys. Lett.* **1982**, *89*, 149.
(25) Mulliken, R. S. *J. Am. Chem. Soc.* **1952**, *74*, 811.
(26) Orgel, L. E.; Mulliken, R. S. *J. Am. Chem. Soc.* **1957**, *79*, 4839.
(27) Strong, R. L.; Rand, S. J.; Britt, J. A. *J. Am. Chem. Soc.* **1960**, *82*, 5053.
(28) Gover, T. A.; Porter, G. *Proc. R. Soc. A (London)* **1961**, *262*, 476.
(29) Fournier de Violet, P.; Bonneau, R.; Joussot-Dubien, J. *Chem. Phys. Lett.* **1973**, *19*, 251.
(30) Grajower, R.; Jortner, J. *J. Am. Chem. Soc.* **1963**, *85*, 512.
(31) Schofield, D. P.; Kjaergaard, H. G. *J. Chem. Phys.* **2004**, *120*, 6930.
(32) Crawford, T. D.; Abrams, M. L.; King, R. A.; Lane, J. R.; Schofield, D. P.; Kjaergaard, H. G. *J. Chem. Phys.* **2006**, *125*, 204302.
(33) Tsai, M.-K.; Kowalski, K.; Valiev, M.; Dupuis, M. *J. Phys. Chem. A* **2007**, *111*, 10478.
(34) Cheng, B.-M.; Chew, E. P.; Liu, C.-P.; Bahou, M.; Lee, Y.-P.; Yung, Y. L.; Gerstell, M. F. *Geophys. Res. Lett.* **1999**, *26*, 3657.
(35) Heller, J. M.; Hamm, R. N.; Birkoff, R. D.; Painter, L. R. *J. Chem. Phys.* **1974**, *60*, 3483.
(36) Page, R. H.; Larkin, R. J.; Shen, Y. R.; Lee, Y. T. *J. Chem. Phys.* **1988**, *88*, 2249.

(37) Smith, J. R.; Kim, J. B.; Lineberger, W. C. *Phys. Rev. A* **1997**, *55*, 2036.
(38) Del Bene, J. E.; Ditchfield, R.; Pople, J. A. *J. Chem. Phys.* **1971**, *55*, 2236.
(39) Foresman, J. B.; Head-Gordon, M.; Pople, J. A.; Frisch, M. J. *J. Phys. Chem.* **1992**, *96*, 135.
(40) Runge, E.; Gross, E. K. U. *Phys. Rev. Lett.* **1984**, *52*, 997.
(41) Casida, M. E. In *Recent Advances in Density Functional Methods*; Chong, D. P., Ed.; World Scientific: Singapore, 1995; Vol. I.
(42) Hirata, S.; Head-Gordon, M. *Chem. Phys. Lett.* **1999**, *314*, 291.
(43) Becke, A. D. *J. Chem. Phys.* **1993**, *98*, 5648.
(44) Lee, C. T.; Yang, W. T.; Parr, R. G. *Phys. Rev. B* **1988**, *37*, 785.
(45) Becke, A. D. *J. Chem. Phys.* **1993**, *98*, 1372.
(46) The NWChem program actually implements only an approximation to the BHandH functional of ref 45. The approximation takes the form $0.5E_X^{HF} + 0.5E_X^{Slater} + 0.5E_C^{PW91LDA}$ for the exchange-correlation energy,
(47) Lynch, B. J.; Fast, P. L.; Harris, M.; Truhlar, D. G. *J. Phys. Chem. A* **2000**, *104*, 4811.
(48) Bylaska, E. J.; de Jong, W. A.; Kowalski, K.; Straatsma, T. P.; Valiev, M.; Wang, D.; Aprà, E.; Windus, T. L.; Hirata, S.; Hackler, M. T.; Zhao, Y.; Fan, P.-D.; Harrison, R. J.; Dupuis, M.; Smith, D. M. A.; Nieplocha, J.; Tipparaju, V.; Krishnan, M.; Auer, A. A.; Nooijen, M.; Brown, E.; Cisneros, G.; Fann, G. I.; Früchtl, H.; Garza, J.; Hirao, K.; Kendall, R.; Nichols, J. A.; Tsemekhman, K.; Wolinski, K.; Anchell, J.; Bernholdt, D.; Borowski, P.; Clark, T.; Clerc, D.; Dachsel, H.; Deegan, M.; Dyall, K.; Elwood, D.; Glendening, E.; Gutowski, M.; Hess, A.; Jaffe, J.; Johnson, B.; Ju, J.; Kobayashi, R.; Kutteh, R.; Lin, Z.; Littlefield, R.; Long, X.; Meng, B.; Nakajima, T.; Niu, S.; Pollack, L.; Rosing, M.; Sandrone, G.; Stave, M.; Taylor, H.; Thomas, G.; van Lenthe, J.; Wong, A.; Zhang, Z. *NWChem, A Computational Chemistry Package for Parallel Computers*, Version 5.0; Pacific Northwest National Laboratory: Richland, WA, 2006.
(49) Schmidt, M. W.; Baldridge, K. K.; Boatz, J. A.; Elbert, S. T.; Gordon, M. S.; Jensen, J. H.; Koseki, S.; Matsunaga, N.; Nguyen, K. A.; Su, S. J.; Windus, T. L.; Dupuis, M.; Montgomery, J. A. *J. Comput. Chem.* **1993**, *14*, 1347.
(50) Ivanic, J. *J. Chem. Phys.* **2003**, *119*, 9364.
(51) Ivanic, J. *J. Chem. Phys.* **2003**, *119*, 9377.
(52) Dalgaard, E.; Monkhorst, H. J. *Phys. Rev. A* **1983**, *28*, 1217.
(53) Stanton, J. F.; Bartlett, R. J. *J. Chem. Phys.* **1993**, *98*, 7029.
(54) Piecuch, P.; Kucharski, S. A.; Kowalski, K.; Musial, M. *Comput. Phys. Commun.* **2002**, *149*, 71.
(55) Kowalski, K.; Piecuch, P. *J. Chem. Phys.* **2004**, *120*, 1715.
(56) Raghavachari, K.; Trucks, G. W.; Pople, J. A.; Head-Gordon, M. *Chem. Phys. Lett.* **1989**, *157*, 479.
(57) Hehre, W. J.; Ditchfield, R.; Pople, J. A. *J. Chem. Phys.* **1972**, *54*, 2257.
(58) Hariharan, P. C.; Pople, J. A. *Theor. Chim. Acta* **1973**, *28*, 213.
(59) Clark, T. C.; Chandrasekhar, J.; Spitznagel, G. W.; von Rague Schleyer, P. *J. Comput. Chem.* **1983**, *4*, 294.
(60) Krishnan, R.; Binkley, J. S.; Seeger, R.; Pople, J. A. *J. Chem. Phys.* **1980**, *72*, 650.
(61) Chipman, D. M. *J. Chem. Phys.* **2005**, *122*, 044111.
(62) Chipman, D. M. *J. Chem. Phys.* **2006**, *124*, 044305.
(63) Chipman, D. M. *J. Chem. Phys.* **2007**, *127*, 194309.
(64) Dunning, T. H. *J. Chem. Phys.* **1989**, *90*, 1007.
(65) Kendall, R. A.; Dunning, T. H.; Harrison, R. J. *J. Chem. Phys.* **1992**, *96*, 6796.
(66) Suppan, P. *J. Photochem. Photobiol., A* **1990**, *50*, 293.
(67) Hush, N. S.; Reimers, J. R. *Chem. Rev.* **2000**, *100*, 775.
(68) Cabral do Couto, P.; Guedes, R. C.; Costa Cabral, B. J.; Martinho Simões, J. A. *J. Chem. Phys.* **2003**, *119*, 7344.
(69) Adamo, C.; Barone, V. *J. Chem. Phys.* **1998**, *108*, 664.
(70) Boys, S. F.; Bernardi, F. *Mol. Phys.* **1970**, *19*, 553.
(71) Du, S. Y.; Francisco, J. S.; Schenter, G. K.; Iordanov, T. D.; Garrett, B. C.; Dupuis, M.; Li, J. *J. Chem. Phys.* **2006**, *124*, 224318.
(72) Hamad, S.; Lago, S.; Mejias, J. A. *J. Phys. Chem. A* **2002**, *106*, 9104.
(73) Gillis, J. R.; Goldman, A.; Stark, G.; Rinsland, C. P. *J. Quant. Spectrosc. Radiat. Transfer* **2001**, *68*, 225.
(74) VandeVondele, J.; Sprik, M. *Phys. Chem. Chem. Phys.* **2005**, *7*, 1363.
(75) Vassilev, P.; Louwerse, M. J.; Baerends, E. J. *Chem. Phys. Lett.* **2004**, *398*, 212.
(76) Vassilev, P.; Louwerse, M. J.; Baerends, E. J. *J. Phys. Chem. B* **2005**, *109*, 23605.
(77) Khalack, J. M.; Lyubartsev, A. P. *J. Phys. Chem. B* **2005**, *109*, 378.

JP807399B